



Magnetic field effects on the quantum spin liquid behaviors of NaYbS₂

Jiangtao Wu^{1†}, Jianshu Li^{2,3†}, Zheng Zhang^{2,3†}, Changle Liu⁴, Yong Hao Gao⁴, Erxi Feng^{5,6}, Guochu Deng⁷, Qingyong Ren¹, Zhe Wang^{8,9}, Rui Chen¹⁰, Jan Embs¹¹, Fengfeng Zhu⁵, Qing Huang¹², Ziji Xiang¹³, Lu Chen¹³, Yan Wu⁶, E.S. Choi¹⁴, Zhe Qu⁸, Lu Li¹³, Junfeng Wang¹⁰, Haidong Zhou^{12,14}, Yixi Su⁵, Xiaoqun Wang¹, Gang Chen^{15,16}, Qingming Zhang^{17,2*} and Jie Ma^{1,10*} 

Abstract

Spin-orbit coupling is an important ingredient to regulate the many-body physics, especially for many spin liquid candidate materials such as rare-earth magnets and Kitaev materials. The rare-earth chalcogenides NaYbCh₂ (Ch = O, S, Se) is a congenial frustrating system to exhibit the intrinsic landmark of spin liquid by eliminating both the site disorders between Na⁺ and Yb³⁺ ions with the big ionic size difference and the Dzyaloshinskii-Moriya interaction with the perfect triangular lattice of the Yb³⁺ ions. The temperature versus magnetic-field phase diagram is established by the magnetization, specific heat, and neutron-scattering measurements. Notably, the neutron diffraction spectra and the magnetization curve might provide microscopic evidence for a series of spin configuration for in-plane fields, which include the disordered spin liquid state, 120° antiferromagnet, and one-half magnetization state. Furthermore, the ground state is suggested to be a gapless spin liquid from inelastic neutron scattering, and the magnetic field adjusts the spin orbit coupling. Therefore, the strong spin-orbit coupling in the frustrated quantum magnet substantially enriches low-energy spin physics. This rare-earth family could offer a good platform for exploring the quantum spin liquid ground state and quantum magnetic transitions.

1 Introduction

Quantum spin liquid (QSL) is a long-range entangled “quantum liquid” state of interacting spins [1–3], which is believed not only to be a platform for obtaining the original driving force of the high-temperature superconductivity but also to be a basic unit for the quantum data storage and computation. Although there has been much theoretical effort on different models of QSL, a firm experimental establishment of this exciting and ex-

otic phase in a real compound is still lacking. Although limited behaviors have been confirmed and actively investigated on a few spin liquid candidate compounds, such as the organic materials [4–7] κ -(BEDT-TTF)₂Cu₂(CN)₃ and EtMe₃Sb[Pd(dmit)₂]₂, kagomé herbertsmithite [8, 9] ZnCu₃(OH)₆Cl₂, the cluster Mott insulator [10, 11] 1T-TaS₂ in the commensurate charge density wave phase, the honeycomb Kitaev materia [12–16], and the pyrochlore spin ice materials [17–27], there is always some unexpected factors observed in these candidate materials, such as the distorted lattice, relatively low-energy scale of the spin interactions, anti-site ionic disordering, and restricted experimental resolution, and the intrinsic magnetic behaviors might be shaded. Therefore, investigating an ideal compound and revealing the intrinsic quantum and magnetic properties related to QSLs is crucial to both material and physics research.

*Correspondence: qmzhang@iphy.ac.cn; jma3@sjtu.edu.cn

¹⁷School of Physical Science and Technology, Lanzhou University, Lanzhou 730000, China

¹Key Laboratory of Artificial Structures and Quantum Control, Shenyang National Laboratory for Materials Science, School of Physics and Astronomy, Tsung-Dao Lee Institute, Shanghai Jiao Tong University, Shanghai 200240, China

Full list of author information is available at the end of the article †Equal contributors

Previously, part of us and many others have worked on a rare-earth triangular lattice magnet YbMgGaO_4 [28–48] where the Yb^{3+} ions form a perfect triangular lattice with spin-orbit-entangled effective spin-1/2 local moments. Thus, YbMgGaO_4 is likely to be the first spin liquid candidate in the strong spin-orbit-coupled Mott-insulators with odd electron fillings [29, 30, 49] and goes beyond the conventional Oshikawa-Hastings-Lieb-Schultz-Mattis theorem [50–53] that requires the U(1) spin rotational symmetry. However, the potential issue of YbMgGaO_4 is the Mg-Ga disorder in the non-magnetic layers. To what extent the non-magnetic disorder in the non-magnetic layer would impact the intrinsic magnetic properties of the system may require further scrutiny. Instead of delving with YbMgGaO_4 , we turn to a different route. This is motivated by the robustness of QSLs and the principle of universality. If the QSL ground state is relevant for YbMgGaO_4 , similar QSL state could likely be realized in other triangular lattice rare-earth magnets. On the other hand, other triangular lattice rare-earth magnets could potentially eliminate the non-magnetic disorder issue that was suggested for YbMgGaO_4 . Indeed, a series of rare-earth chalcogenides was recently identified [54, 56–67] as candidates for QSLs, and apparently, there is no structural disorder like the Mg/Ga ions in YbMgGaO_4 . Therefore, we combine the experimental measurements and theoretical analysis and propose NaYbS_2 likely to be a gapless QSL candidate. The field- and temperature-dependence of magnetization, specific heat, neutron diffraction, and inelastic neutron scattering measurements demonstrate several field-induced magnetic transitions in this QSL ground state system. Moreover, we provide extra theoretical results and suggestions for further experimental verification of the QSL state in the isostructural compounds.

2 Samples and experimental techniques

The polycrystalline and single crystals of NaYbS_2 were synthesized by the high-temperature solid-state reaction and the NaCl-flux method, respectively [54]. Around 0.5 g single crystals of NaYbS_2 were co-aligned in the (HHL) scattering plane on a copper plate, and the single-crystal neutron diffraction data were collected at the Australia Nuclear Science and Technology Organisation (ANSTO), using a cold neutron triple-axis diffractometer, Sika [55]. An 8 T vertical magnetic field cryostat with a dilution refrigerator insert was applied to collect magnetic field data at 0 T, 3 T, 4 T, 5 T, and 8 T at 0.1 K. The magnetic field was applied along $[1 \ -1 \ 0]$, and the data were collected with final energy as $E_f \sim 5$ meV. Rietveld refinement was performed with the SARA software and the magnetic symmetry approach at the Bilbao Crystallographic Server. The fitted data are shown in Fig. 1 at 300 K and 1.6 K. The inelastic neutron-scattering powder data were collected at the Swiss Spallation Neutron

Source (SINQ), the Paul Scherrer Institut (PSI), using a disc chopper spectrometer, FOCUS, in a 10 T magnetic field with a dilution insert. Incident neutrons with 5 Å wavelength were used with the medium-resolution chopper setting.

Specific heat measurements were performed for sintered pellets of NaYbS_2 down to 0.3 K at zero-field on a physical property measurement system (PPMS, Quantum Design), and the He-3 refrigerator insert was applied for temperatures below 1.8 K. Moreover, data under 3 T, 4 T, 5 T, 6 T, 7 T, 8 T, and 9 T applied fields were also collected. The magnetic signal of specific heat was determined by subtracting the data of non-magnetic compound NaLuS_2 between 1.8 K and 30 K. The calculated magnetic entropy was obtained by integrating C_{mag}/T between 0.3 K and 20 K.

Magnetic properties were measured by using several different instruments. Isothermal DC magnetization up to 9 T was collected on a PPMS with a vibrating sample magnetometer insert, and isothermal AC susceptibility in applied fields up to 7 T from 0.5 K to 20 K was obtained on a magnetic property measurement system (MPMS3, Quantum Design). The DC magnetic susceptibilities versus H up to 18 T at 0.8 K were collected at Wuhan National High Magnetic Field Center. Torque magnetometry was performed at the University of Michigan using a self-built capacitive cantilever setup mounted inside a dilution refrigerator.

3 Neutron diffraction and magnetic structure

The rare-earth ions in the chalcogenides NaYbCh_2 ($\text{Ch} = \text{O}, \text{S}, \text{Se}$) have an ideal triangular lattice structure with the magnetic Yb^{3+} ions localized at the center of chalcogenide octahedra, Fig. 1(a), and the Yb^{3+} triangular layers are well separated by the non-magnetic NaCh_6 octahedra. Since the difference between the Na^+ and Yb^{3+} ionic sizes is large, the anti-site disorder is eliminated. The single-crystal XRD data have confirmed that the anti-site disorder between them is less than 4%. NaYbCh_2 has a perfect triangular lattice, and the intrinsic properties of the QSL, if there exists any, would be more clearly presented. We perform the neutron powder diffraction on NaYbS_2 and compare the results at 50 mK and 300 mK, Fig. 1(b). From the labeled lattice reflections, the overplotting agreement suggests no long-range magnetic ordering down to 50 mK in this system. The space groups of NaYbCh_2 is $R\bar{3}m$, which is same as YbMgGaO_4 and different to the P -lattice type triangular oxides with a rotation axis C_3 or C_6 of the Z_3 symmetry, such as $\text{Ba}_3\text{CoSb}_2\text{O}_9$ and $\text{K}_2\text{Mn}_3(\text{VO}_4)_2\text{CO}_3$ [68, 69]. Meanwhile, the external magnetic field could break the degenerated ground state and induce complicated magnetic structures ([57] and see Additional file 1).

To determine the magnetic structure of new phases under the field, single-crystal neutron diffraction was applied,

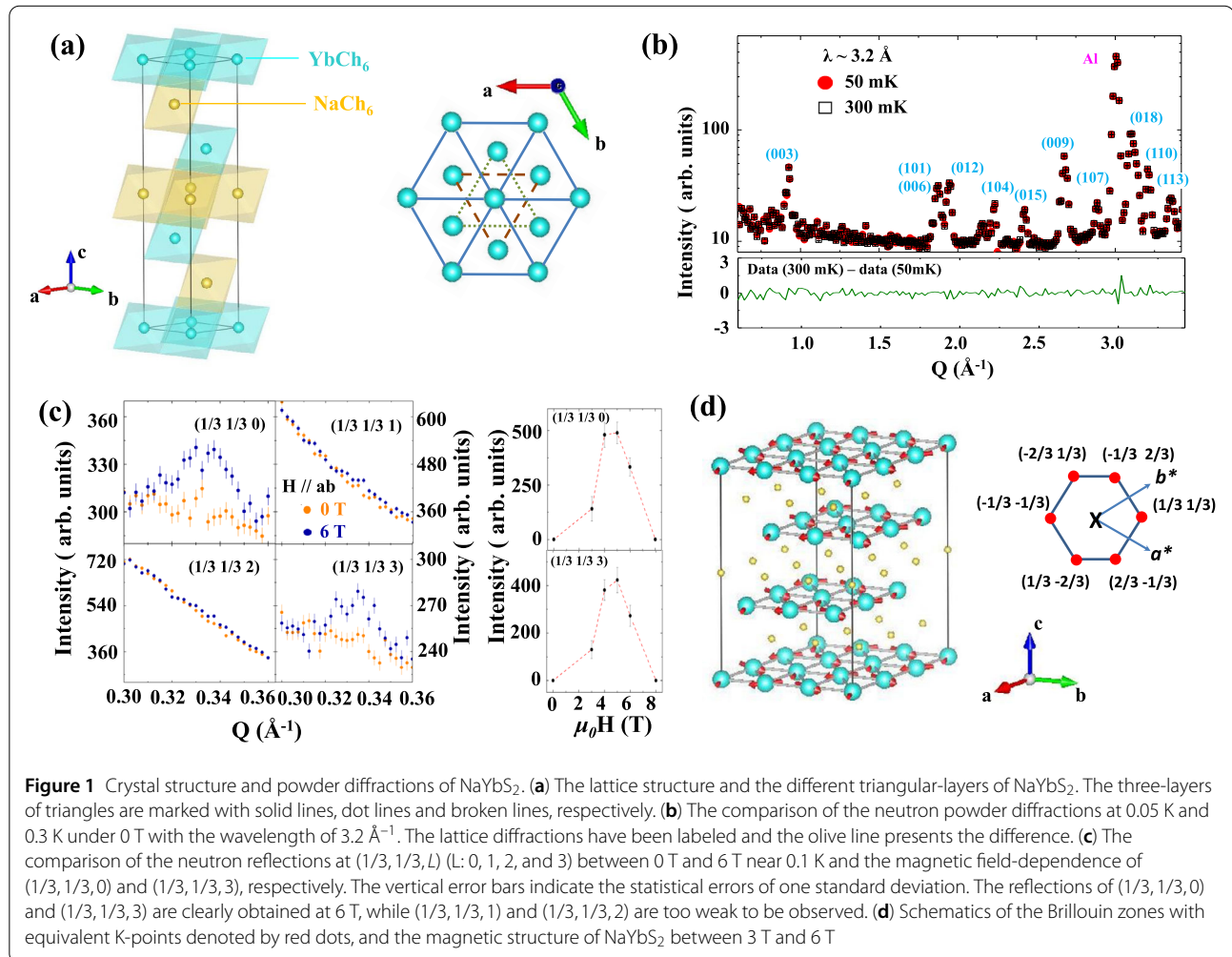


Figure 1 Crystal structure and powder diffractions of NaYbS₂. **(a)** The lattice structure and the different triangular-layers of NaYbS₂. The three-layers of triangles are marked with solid lines, dot lines and broken lines, respectively. **(b)** The comparison of the neutron powder diffractions at 0.05 K and 0.3 K under 0 T with the wavelength of 3.2 \AA . The lattice diffractions have been labeled and the olive line presents the difference. **(c)** The comparison of the neutron reflections at $(1/3, 1/3, L)$ ($L: 0, 1, 2, \text{ and } 3$) between 0 T and 6 T near 0.1 K and the magnetic field-dependence of $(1/3, 1/3, 0)$ and $(1/3, 1/3, 3)$, respectively. The vertical error bars indicate the statistical errors of one standard deviation. The reflections of $(1/3, 1/3, 0)$ and $(1/3, 1/3, 3)$ are clearly obtained at 6 T, while $(1/3, 1/3, 1)$ and $(1/3, 1/3, 2)$ are too weak to be observed. **(d)** Schematics of the Brillouin zones with equivalent K-points denoted by red dots, and the magnetic structure of NaYbS₂ between 3 T and 6 T

Fig. 1(c). Although up-up-down (uud) plateau phase has been reported to be induced by the magnetic field in the isostructure NaYbO₂ [57] and NaYbS₂ has the similar powder neutron diffraction spectra except an extra reflection at $q \approx 1.2429 \text{ \AA}^{-1}$ (see Additional file 1), surprisingly, the reflections of $(1/3, 1/3, 1)$ and $(1/3, 1/3, 2)$ were too weak to be observed under the field, which is different to the powder data of NaYbO₂ ([57] and see Additional file 1). Based on the program SARAh [70] and the magnetic symmetry approach at the Bilbao Crystallographic Server [71], the magnetic Yb³⁺ ions spiral upwards with a 120° state and the equivalent reflections of $(2/3, -1/3, 1)$ and $(2/3, -1/3, -2)$ are instead of $(1/3, 1/3, 1)$ and $(1/3, 1/3, 2)$, Fig. 1(d). Therefore, the magnetic wave vector is $(1/3, 1/3, 0)$. As the magnetic field increased, the reflections of $(1/3, 1/3, 0)$ and $(1/3, 1/3, 3)$ disappeared above 8 T. Since this high field phase does not have the wave vector of $(1/3, 1/3)$ in ab -plane, it is disappointed to minimize the possibility of reported *uud* plateau in NaYbO₂.

Compared to the $M(H)$ measurements with the van Vleck correction, the saturated magnetization is $1.0\mu_B$ per

Yb³⁺ ion and the moment of the intermediate phase is $0.5\mu_B$ per Yb³⁺ ion with a constant dM/dH , Fig. 2(a). The plateau phase has been predicted by Ye et al. as an up-up-up-down (uuud) state and breaks either Z_3 orientational symmetry or Z_4 sublattice symmetry with the competition of the magnetic field and quantum fluctuations [72]. Therefore, the subsequent state above the 120° state is an uuud state, which has been realized on the triangular lattice antiferromagnet Fe_{1/3}NbS₂ [73] and YbMgGaO₄ [74], and the stabilization of such a state requires further neighbor exchange interaction. A recent study on the diamond lattice antiferromagnet LiYbO₂ does suggest the importance of the second neighbor exchange interaction [75]. Moreover, the magnetic wave vector of *uuud* phase shifts from $(1/3, 1/3, 0)$ to $(0, 1/2, 0)$ in AgNiO₂ [76, 77]. On further increasing the magnetic field, the *uuud* phase undergoes a second-order phase transition to a high-field oblique phase, commonly to be observed in triangular lattices [72].

4 Thermodynamic data at finite temperature and phase diagram

To reveal the magnetic phases in detail, the DC and AC magnetizations and the torque magnetometry were measured. For zero field, the Curie-Weiss temperatures of $\Theta_{CW,\perp} = -13.5$ K and $\Theta_{CW,\parallel} = -4.5$ K for the in-plane and out-of-plane susceptibility measurements [56] present the related frustration parameters as $f > |\Theta_{CW,\perp}|/(0.05 \text{ K}) \approx 270$ for the in-plane value and $f > |\Theta_{CW,\parallel}|/(0.05 \text{ K}) \approx 90$ for the out-of-plane value. Meanwhile, the larger in-plane Curie-Weiss temperature expects to enhance the spin correlation between the in-plane spin components and contribute mostly to the diffusive scattering peak. The exchange energy scale of NaYbS_2 is a couple times larger than the ones in YbMgGaO_4 , consistent with the enhanced Curie-Weiss temperatures. This advantage allows a broader temperature window to explore the QSL physics in this system. Furthermore, it is noted that the magnetic susceptibility in the zero field limit is constant. Although it seems to be consistent with a spinon Fermi surface state, this is expected from the fact that the total magnetization is not a conserved quantity. Thus, the constant spin susceptibility cannot be used to identify the QSL ground state for this material and other materials. Unlike NaYbO_2 , NaYbS_2 demonstrates quite rich phases with a higher saturated magnetization field (up to ~ 16.0 T), Fig. 2: there are four transition fields for DC susceptibility at 0.8 K, ~ 3.3 T, 6.1 T, 10.2 T, and 14.8 T, respectively, and are con-

sistent with the transition fields by the AC susceptibility very well (see Additional file 1). Figure 2(b) presented the torque magnetometry measurements by applying the field in the *ab*-plane. The dM/dH curves between 30 mK and 600 mK show two peaks on the lower and upper critical fields. As the temperature increases, this derivative becomes weaker and finally disappears around $T = 1$ K. Finally, the sublattice spins are aligned along the applied field and saturated.

The low-temperature specific heat measurements on NaYbS_2 were performed down to 0.3 K at zero-field, Fig. 2(c). As the neutron powder diffraction measurement, no signature of magnetic transition is observed, and a broad peak occurs at about 1 K, a typical phenomenon of the QSL candidate materials. The lattice phonon contribution to the specific heat is obtained from the isostructural non-magnetic material NaLuS_2 and could be almost negligible below 3 K, Fig. 2(c). The entropy release for NaYbS_2 from 0.3 K to 20 K saturates up to 92% of the $R \ln 2$ entropy (where R is the ideal gas constant), and an effective spin-1/2 description of the Yb^{3+} local moments is obtained. Unlike YbMgGaO_4 , C_p/T of NaYbS_2 does not diverge at low temperatures, while the divergence in YbMgGaO_4 is interpreted as the signature of U(1) gauge fluctuations [29, 30]. The intercept of C_p/T on the $T = 0$ axis is slightly larger than the one for NaYbO_2 , and the specific heat fits well with a T^2 behavior below 0.7 K, the inset in Fig. 2(c), which is consistent with a gapless QSL and the Lorentz invariance

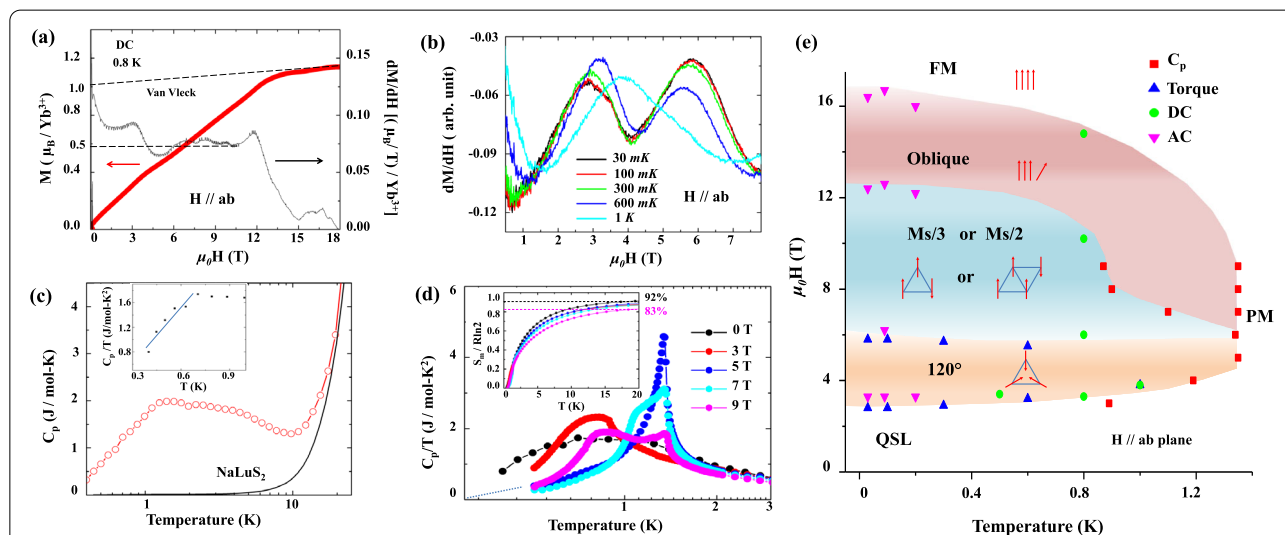


Figure 2 The magnetization, torque magnetometry, specific heat and the phase diagram with $H//ab$ -plane of NaYbS_2 . (a) DC magnetic susceptibility versus H and the related derivative dM/dH versus H at 0.8 K. The anomaly fields are ~ 3.3 T, 6.1 T, 10.2 T and 14.8 T. The dash lines present the saturated magnetization of $1.0\mu_B$ per Yb ion with van Vleck correction and the intermediate $\text{Ms}/2$ anomaly-phase of $0.5\mu_B$ per Yb ion, respectively. (b) The temperature-dependence of the torque magnetometry in DC field. The fields marked by the black arrows are suggested as the magnetic phase transition fields. (c) The specific heat of NaYbS_2 and NaLuS_2 , respectively. Inset presents the linear relationship of C_p/T vs T below 0.7 K. (d) The magnetic field-dependence of specific heat divided by T as a function of temperature and the related magnetic entropy. (e) The proposed magnetic phase diagram of temperature versus magnetic field for NaYbS_2 with different techniques

guarantees. A residual density of states that contribute to the small intercept could be regarded [78] as the tail of the contributions of Yb^{3+} nuclear spin and becomes more and more significant below 0.1 K.

As the external magnetic field is applied, the specific heat demonstrates a series of highly tunable states, which relate to the quantum and thermal fluctuations, Fig. 2(d): a broad peak starts to be observed at 3 T, then a sharp peak appears at 5 T around ~ 1.3 K and turns to be suppressed gradually with the increasing field. Finally another broad peak is split from the sharp peak and shifts to the lower temperature at 7 T. Those transitions could also be recognized by the magnetic entropy, which decreases from 92% (0 T) to 86% (3 T), then increases 88% (5 T), and drops again to 83% (9 T). Meanwhile, the low-temperature specific heat below the peak temperature is strongly suppressed, and C_p/T actually goes to zero in the zero temperature limit. Hence, the magnetic field breaks the QSL ground state and induces a range of intermediate states before the magnetic Yb^{3+} ions in NaYbS_2 are fully saturated.

The temperature versus magnetic field diagram is plotted in Fig. 2(e). The phase transitions are determined by combining different techniques, and the various exotic states from 120° to the $uuud$ Ms/2 anomaly-phase to oblique phases were decided. Especially, the thermal effect is realized in the system even at low temperatures, ~ 0.8 K, with the S-shape transition between the Ms/2- or Ms/3-anomaly phase and oblique phases.

5 Inelastic neutron scattering and gapless spin liquid

We perform the inelastic neutron scattering (INS) measurements on NaYbS_2 both at $H = 0$ T and 6 T at 50 mK. This measurement contains the dynamical energy-momentum information about the magnetic excitations in the system. In Fig. 3(a), highly dispersive signals are revealed. It is proposed a U(1) spinon Fermi surface spin liquid in YbMgGaO_4 with a clear V-shape at Γ point [30]. Several key features can be lost for the powder sample of NaYbS_2 due to the lack of angular momentum information. However, there still exists a cone feature that can be distinguished at $|\mathbf{Q}| \approx 1.24 \text{ \AA}^{-1}$ from Fig. 3(a), which should correspond to the cone-like feature of the Dirac spin liquid. The inter-Dirac cone scattering and intra-Dirac cone scattering processes would present these characters at low energies. Meanwhile, for the spinon Fermi surface states, a large amount of low-energy intensity is expected in a wider momentum range, which is clearly incompatible with the experimental data. For example, NaYbSe_2 [79] is a quantum spin liquid candidate with spinon Fermi surface states. With magnetic field $H = 6$ T, as depicted in Fig. 3(b) and the insets of constant-energy and -moment cuts in Fig. 3(c) and (d), the low-energy spectral weight is mostly transferred to higher energies, consistent with specific heat data

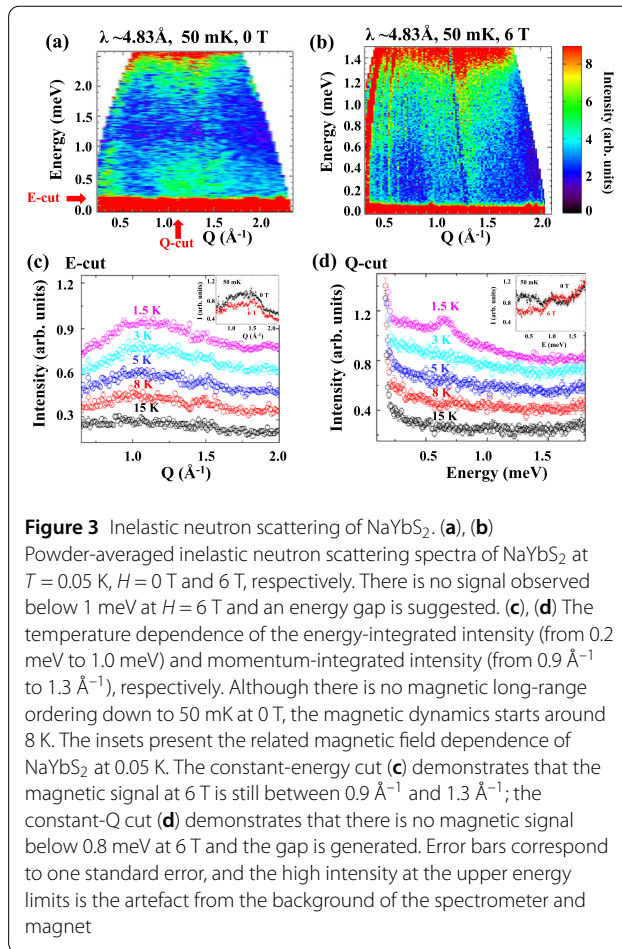


Figure 3 Inelastic neutron scattering of NaYbS_2 . (a), (b) Powder-averaged inelastic neutron scattering spectra of NaYbS_2 at $T = 0.05$ K, $H = 0$ T and 6 T, respectively. There is no signal observed below 1 meV at $H = 6$ T and an energy gap is suggested. (c), (d) The temperature dependence of the energy-integrated intensity (from 0.2 meV to 1.0 meV) and momentum-integrated intensity (from 0.9 \AA^{-1} to 1.3 \AA^{-1}), respectively. Although there is no magnetic long-range ordering down to 50 mK at 0 T, the magnetic dynamics starts around 8 K. The insets present the related magnetic field dependence of NaYbS_2 at 0.05 K. The constant-energy cut (c) demonstrates that the magnetic signal at 6 T is still between 0.9 \AA^{-1} and 1.3 \AA^{-1} ; the constant-Q cut (d) demonstrates that there is no magnetic signal below 0.8 meV at 6 T and the gap is generated. Error bars correspond to one standard error, and the high intensity at the upper energy limits is the artefact from the background of the spectrometer and magnet

that this field-induced state should be gapped due to the anisotropic spin interactions between the Yb^{3+} local moments, which is different to NaYbO_2 with the bigger S^2 -ion on the Ch-site. Moreover, the temperature dependence of the energy- and moment-integrated intensities, Fig. 3(c) and (d), clearly presented that the V-shape magnetic signals start to be observed around 8 K.

Furthermore, NaYbS_2 was also suggested as a gapless quantum spin liquid by longitudinal field (LF) muon spin relaxation (μSR) [80]. At 0.1 K, an indicator as the spin relaxation rate, λ_{LF} , was applied to describe the spin dynamics and obtained from LF- μSR experimental data of NaYbS_2 . As the magnetic field increased to 1000 G, λ_{LF} was almost close to zero, significantly different from the LF- μSR spin relaxation rate λ_{LF} of quantum spin liquids with spinon Fermi surface state. For example, the quantum spin liquid material NaYbSe_2 demonstrated a spinon Fermi surface state [79], and the spin relaxation rate λ_{LF} maintained a constant value of $\sim 0.2 \mu\text{s}^{-1}$ at 0.1 K and the magnetic field of 1000 G [80]. Although both NaYbS_2 and NaYbSe_2 had magnetic ground states with quantum spin liquid states, and the crystallographic structures were close, the spinon excitation characteristics were signifi-

cantly different. Therefore, the substitution of the oxychloride element effect was clearly demonstrated, and the crystal electric field played an important role in regulating quantum spin liquids [81].

6 Summary

Comparing to NaYbO_2 , the bigger S^{2-} ion on the Ch-site not only prevents crystallographic site-mixing, but also increases the interlayer distances via the mediating cation, therefore the Yb^{3+} layer distance along the c axis is reduced significantly in NaYbS_2 with the slightly larger a axis and leads to the c/a ratio for NaYbS_2 (5.1) is more closer to YbMgGaO_4 (7.4) than NaYbO_2 (4.9). Rather than a pure two-dimensional model with anisotropic exchanges, a more precise theoretical analysis should naturally include other factors, such as the interlayer couplings [57]. Although the spins in the oxide are expected to be more localized than in sulfide, the quantum effects from both spin- and thermal-fluctuations in the latter are more complicated. Additionally, the ground state of NaYbS_2 can be driven into a magnetically ordered state in intermediate magnetic fields. Due to the strong easy-plane exchange anisotropy of NaYbS_2 , the numerical studies suggest a canted 120° state or an incommensurate state rather than an uud state in NaYbO_2 , which is also confirmed by the magnetization and neutron diffraction measurements.

Our experiments demonstrate that the nearly ideal triangular lattice of Yb ions in strongly spin-orbit-coupled materials NaYbCh_2 can realize various exotic ground states. Especially, both the thermodynamic and the neutron scattering measurements suggest NaYbS_2 realizes a gapless spin liquid state. According to the fermion doubling theorem, there cannot be a single Dirac cone in a lattice system, and the cones must at least come in pairs. INS experiments measure the dynamical spin structural factor, which corresponds to the particle-hole pair of spinon excitations, and the intra-cone scattering will contribute to low energy spin excitations near Γ point. In contrast, the inter-cone scattering corresponds to low energy spin excitations at finite momentum [30, 49]. Furthermore, the scenario of staggered π -flux Dirac spin liquid would double the unit cell of spinons. This results in an enhanced periodicity of the dynamical spin structure factor despite the lack of magnetic ordering, which can be identified as a sharp feature to distinguish this peculiar fractionalized state from trivial spin glass. Although the density-of-state decided the momentum-dependence of the spin dynamics and no gap above 0.1 meV, the clear feature of enhanced periodicity is smeared out due to lack of angular resolution, and more experimental efforts on NaYbS_2 single crystals are highly desired to distinguish if this system really hosts this π -flux gapless (or Dirac) spin liquid state.

Supplementary information

Supplementary information accompanies this paper at <https://doi.org/10.1007/s44214-022-00011-z>.

Additional file 1. Supplementary information (PDF 315 kB)

Acknowledgements

J.M. and X.Q.W. acknowledge additional support from a Shanghai talent program. Q.M.Z. acknowledges the support from Users with Excellence Program of Hefei Science Center and High Magnetic Field Facility, CAS and the synergetic Extreme Condition User Facility (SECUF), CAS. Q.H. and H.Z. thank the support from NSF-DMR-2003117. F.Z., E.F. and Y.S. thank the support of the OCPH-HGF Postdoctoral Fellowship. The torque magnetometry work at Michigan was supported by the U.S. Department of Energy (DOE) under Award No. DE-SC0020184. A portion of this work was performed at the National High Magnetic Field Laboratory, which is supported by the National Science Foundation Cooperative Agreement No. DMR-1644779 and the State of Florida.

Funding

This work is supported by the Ministry of Science and Technology of China (Grant No. 2022YFA1402700, 2018YFGH000095), the NSF of China (Grant No. U2032213, 11774223, 12274186, 11774352, 11974244, U1832214, and U1932215), the interdisciplinary program Wuhan National High Magnetic Field Center (Grant No. WHMFC 202122), Huazhong University of Science and Technology, and the Research Grants Council of Hong Kong with General Research Fund Grant No. 17303819 and the Strategic Priority Research Program of the Chinese Academy of Sciences (Grant No. XDB33010100). Open Access funding provided by Shanghai Jiao Tong University.

Availability of data and materials

All data generated or analyzed during this study are included in this article and its supplementary information files.

Declarations

Competing interests

The authors declare no competing interests.

Author contribution

QMZ and JM conducted the study. JSL and ZZ grew NaYbS_2 polycrystalline samples and single crystals. GCD, YW and EXF carried out the neutron powder diffraction of NaYbS_2 and analyzed the data. ZW, ZQ, RC, JFW, QH, ESC, and HDZ performed magnetization measurements. ZX, LC and LL performed torque magnetometry measurements. JTW, QH, HDZ and JM performed specific heat measurements. JTW, QR, FFZ, EXF, JE and ES carried out inelastic neutron scattering of NaYbS_2 and analyzed the data. GC performed the Monte Carlo calculation of the proposed spin model. JTW, ZZ, GC, QMZ, and JM prepared the manuscript and the supplementary materials. All authors read and approved the final manuscript.

Author details

¹Key Laboratory of Artificial Structures and Quantum Control, Shenyang National Laboratory for Materials Science, School of Physics and Astronomy, Tsung-Dao Lee Institute, Shanghai Jiao Tong University, Shanghai 200240, China. ²Beijing National Laboratory for Condensed Matter Physics, Institute of Physics, Chinese Academy of Sciences, Beijing 100190, China. ³Department of Physics, Renmin University of China, Beijing 100872, China. ⁴State Key Laboratory of Surface Physics and Department of Physics, Fudan University, Shanghai 200433, China. ⁵Jülich Centre for Neutron Science (JCNS) at Heinz Maier-Leibnitz Zentrum (MLZ), Forschungszentrum Jülich, Lichtenbergstrasse 1, 85747 Garching, Germany. ⁶Neutron Scattering Division, Oak Ridge National Laboratory, Oak Ridge, Tennessee 37831, USA. ⁷Australian Centre for Neutron Scattering, Australian Nuclear Science and Technology Organisation, New Illawarra Road, Lucas Heights, NSW 2234, Australia. ⁸Anhui Key Laboratory of Condensed Matter Physics at Extreme Conditions, High Magnetic Field Laboratory, Chinese Academy of Sciences, Hefei, Anhui, 230031, China. ⁹University of Science and Technology of China, Hefei, Anhui 230026, China. ¹⁰Wuhan National High Magnetic Field Center, Huazhong University of Science

and Technology, Wuhan 430074, China. ¹¹Laboratory for Neutron Scattering and Imaging, Paul Scherrer Institute, CH-5232 Villigen, Switzerland. ¹²Department of Physics and Astronomy, University of Tennessee, Knoxville, Tennessee 37996, USA. ¹³Department of Physics, University of Michigan, Ann Arbor, 450 Church Street, Ann Arbor, Michigan 48109, USA. ¹⁴National High Magnetic Field Laboratory, Florida State University, Tallahassee, FL 32310, USA. ¹⁵Department of Physics and HKU-UCAS Joint Institute for Theoretical and Computational Physics at Hong Kong, The University of Hong Kong, Hong Kong, China. ¹⁶Collaborative Innovation Center of Advanced Microstructures, Nanjing University, Nanjing, 210093, China. ¹⁷School of Physical Science and Technology, Lanzhou University, Lanzhou 730000, China.

Publisher's Note

Springer Nature remains neutral with regard to jurisdictional claims in published maps and institutional affiliations.

Received: 16 September 2022 Revised: 4 November 2022

Accepted: 7 November 2022 Published online: 17 November 2022

References

- Lee PA (2008) An end to the drought of quantum spin liquids. *Science* 321:1306–1307
- Balents L (2010) Spin liquids in frustrated magnets. *Nature* 464:199–208
- Savary L, Balents L (2016) Quantum spin liquids: a review. *Rep Prog Phys* 80:016502
- Shimizu Y, Miyagawa K, Kanoda K, Maesato M, Saito G (2003) Spin liquid state in an organic Mott insulator with a triangular lattice. *Phys Rev Lett* 91:107001
- Yamashita S, Nakazawa Y, Oguni M, Oshima Y, Nojiri H, Shimizu Y, Miyagawa K, Kanoda K (2008) Thermodynamic properties of a spin-1/2 spin-liquid state in a κ -type organic salt. *Nat Phys* 4:459–462
- Itou T, Oyamada A, Maegawa S, Tamura M, Kato R (2007) Spin-liquid state in an organic spin-1/2 system on a triangular lattice, $\text{EtMe}_3\text{Sb}[\text{Pd}(\text{dmit})_2]_2$. *J Phys Condens Matter* 19:145247
- Itou T, Oyamada A, Maegawa S, Tamura M, Kato R (2008) Quantum spin liquid in the spin-1/2 triangular antiferromagnet $\text{EtMe}_3\text{Sb}[\text{Pd}(\text{dmit})_2]_2$. *Phys Rev B* 77:104413
- Helton JS, Matan K, Shores MP, Nytko EA, Bartlett BM, Yoshida Y, Takano Y, Suslov A, Qiu Y, Chung J-H, Nocera DG, Lee YS (2007) Spin dynamics of the spin-1/2 kagome lattice antiferromagnet $\text{ZnCu}_3(\text{OH})_6\text{Cl}_2$. *Phys Rev Lett* 98:107204
- Han T-H, Helton JS, Chu S, Nocera DG, Rodriguez-Rivera JA, Broholm C, Lee YS (2012) Fractionalized excitations in the spin-liquid state of a kagome-lattice antiferromagnet. *Nature* 492:406–410
- He W-Y, Xu XY, Chen G, Law KT, Lee PA (2018) Spinon Fermi surface in a cluster Mott insulator model on a triangular lattice and possible application to 1T-TaS₂. *Phys Rev Lett* 121:046401
- Law KT, Lee PA (2017) 1T-TaS₂ as a quantum spin liquid. *Proc Natl Acad Sci* 114:6996–7000
- Kasahara Y, Sugii K, Ohnishi T, Shimozawa M, Yamashita M, Kurita N, Tanaka H, Nasu J, Motome Y, Shibauchi T, Matsuda Y (2018) Unusual thermal Hall effect in a Kitaev spin liquid candidate α -RuCl₃. *Phys Rev Lett* 120:217205
- Banerjee A, Bridges CA, Yan J-Q, Aczel AA, Li L, Stone MB, Granroth GE, Lumsden MD, Yiu Y, Knolle J, Bhattacharjee S, Kovrizhin DL, Moessner R, Tennant DA, Mandrus DG, Nagler SE (2016) Proximate Kitaev quantum spin liquid behaviour in a honeycomb magnet. *Nat Mater* 15:733–740
- Banerjee A, Yan J, Knolle J, Bridges CA, Stone MB, Lumsden MD, Mandrus DG, Tennant DA, Moessner R, Nagler SE (2017) Neutron scattering in the proximate quantum spin liquid α -RuCl₃. *Science* 356:1055–1059
- Kasahara Y, Ohnishi T, Mizukami Y, Tanaka O, Ma S, Sugii K, Kurita N, Tanaka H, Nasu J, Motome Y, Shibauchi T, Matsuda Y (2018) Majorana quantization and half-integer thermal quantum Hall effect in a Kitaev spin liquid. *Nature* 559:227–231
- Plumb KW, Clancy JP, Sandilands LJ, Shankar VV, Hu YF, Burch KS, Kee H-Y, Kim Y-J (2014) α -RuCl₃: a spin-orbit assisted Mott insulator on a honeycomb lattice. *Phys Rev B* 90:041112
- Molavian HR, Gingras MJP, Canals B (2007) Dynamically induced frustration as a route to a quantum spin ice state in $\text{Tb}_2\text{Ti}_2\text{O}_7$ via virtual crystal field excitations and quantum many-body effects. *Phys Rev Lett* 98:157204
- Ross KA, Savary L, Gaulin BD, Balents L (2011) Quantum excitations in quantum spin ice. *Phys Rev X* 1:021002
- Gingras MJP, McClarty PA (2014) Quantum spin ice: a search for gapless quantum spin liquids in pyrochlore magnets. *Rep Prog Phys* 77:056501
- Sibille R, Gauthier N, Yan H, Hatnean MC, Ollivier J, Winn B, Filges U, Balakrishnan G, Kenzelmann M, Shannon N, Fennell T (2018) Experimental signatures of emergent quantum electrodynamics in $\text{Pr}_2\text{Hf}_2\text{O}_7$. *Nat Phys* 14:711–715
- Tokiwa Y, Yamashita T, Terazawa D, Kimura K, Kasahara Y, Onishi T, Kato Y, Halim M, Gegenwart P, Shibauchi T, Nakatsuji S, Moon E-G, Matsuda Y (2018) Discovery of emergent photon and monopoles in a quantum spin liquid. *J Phys Soc Jpn* 87:064702
- Petit S, Lhotel E, Guitteny S, Florea O, Robert J, Bonville P, Mirebeau I, Ollivier J, Mutka H, Ressouche E, Decorse C, Hatnean MC, Balakrishnan G (2016) Antiferroquadrupolar correlations in the quantum spin ice candidate $\text{Pr}_2\text{Zr}_2\text{O}_7$. *Phys Rev B* 94:165153
- Chen G (2016) "magnetic monopole" condensation of the pyrochlore ice U(1) quantum spin liquid: application to $\text{Pr}_2\text{Ir}_2\text{O}_7$ and $\text{Yb}_2\text{Ti}_2\text{O}_7$. *Phys Rev B* 94:205107
- MacLaughlin DE, Bernal OO, Shu L, Ishikawa J, Matsumoto Y, Wen J-J, Mourigal M, Stock C, Ehlers G, Broholm CL, Machida Y, Kimura K, Nakatsuji S, Shimura Y, Sakakibara T (2015) Unstable spin-ice order in the stuffed metallic pyrochlore $\text{Pr}_{2+x}\text{Ir}_{2-x}\text{O}_{7-\delta}$. *Phys Rev B* 92:054432
- Sibille R, Lhotel E, Pomjakushin V, Baines C, Fennell T, Kenzelmann M (2015) Candidate quantum spin liquid in the Ce^{3+} pyrochlore stannate $\text{Ce}_2\text{Sn}_2\text{O}_7$. *Phys Rev Lett* 115:097202
- Gaudet J, Smith EM, Dudemaine J, Beare J, Buhariwalla CRC, Butch NP, Stone MB, Kolesnikov AI, Xu G, Yahne DR, Ross KA, Marjerrison CA, Garrett JD, Luke GM, Bianchi AD, Gaulin BD (2019) Quantum spin ice dynamics in the dipole-octupole pyrochlore magnet $\text{Ce}_2\text{Zr}_2\text{O}_7$. *Phys Rev Lett* 122:187201
- Gao B, Chen T, Tam DW, Huang C-L, Sasmal K, Adroja DT, Ye F, Cao H, Sala G, Stone MB, Baines C, Verezhak JAT, Hu H, Chung J-H, Xu X, Cheong S-W, Nallaiyan M, Spagna S, Maple MB, Nevidomskyy AH, Morosan E, Chen G, Dai P (2019) Experimental signatures of a three-dimensional quantum spin liquid in effective spin-1/2 $\text{Ce}_2\text{Zr}_2\text{O}_7$ pyrochlore. *Nat Phys* 15:1052–1057
- Li Y, Liao H, Zhang Z, Li S, Jin F, Ling L, Zhang L, Zou Y, Pi L, Yang Z, Wang J, Wu Z, Zhang Q (2015) Gapless quantum spin liquid ground state in the two-dimensional spin-1/2 triangular antiferromagnet YbMgGaO_4 . *Sci Rep* 5:16419
- Li Y, Chen G, Tong W, Pi L, Liu J, Yang Z, Wang X, Zhang Q (2015) Rare-Earth triangular lattice spin liquid: a single-crystal study of YbMgGaO_4 . *Phys Rev Lett* 115:167203
- Shen Y, Li Y-D, Wo H, Li Y, Shen S, Pan B, Wang Q, Walker HC, Steffens P, Boehm M, Hao Y, Quintero-Castro DL, Harriger LW, Frontzek MD, Hao L, Meng S, Zhang Q, Chen G, Zhao J (2016) Evidence for a spinon Fermi surface in a triangular-lattice quantum-spin-liquid candidate. *Nature* 540:559–562
- Li Y-D, Wang X, Chen G (2016) Anisotropic spin model of strong spin-orbit-coupled triangular antiferromagnets. *Phys Rev B* 94:035107
- Li Y, Adroja D, Biswas PK, Baker PJ, Zhang Q, Liu J, Tsirlin AA, Gegenwart P, Zhang Q (2016) Muon spin relaxation evidence for the U(1) quantum spin-liquid ground state in the triangular antiferromagnet YbMgGaO_4 . *Phys Rev Lett* 117:097201
- Xu Y, Zhang J, Li YS, Yu YJ, Hong XC, Zhang QM, Li SY (2016) Absence of magnetic thermal conductivity in the quantum spin-liquid candidate YbMgGaO_4 . *Phys Rev Lett* 117:267202
- Li Y-D, Chen G (2017) Detecting spin fractionalization in a spinon Fermi surface spin liquid. *Phys Rev B* 96:075105
- Li Y, Adroja D, Voneshen D, Bewley RI, Zhang Q, Tsirlin AA, Gegenwart P (2017) Nearest-neighbour resonating valence bonds in YbMgGaO_4 . *Nat Commun* 8:15814
- Li Y, Adroja D, Bewley RI, Voneshen D, Tsirlin AA, Gegenwart P, Zhang Q (2017) Crystalline electric-field randomness in the triangular lattice spin-liquid YbMgGaO_4 . *Phys Rev Lett* 118:107202
- Tóth S, Rols K, Wildes AR, Rüegg C (2017) Strong exchange anisotropy in YbMgGaO_4 from polarized neutron diffraction. [arXiv:1705.05699](https://arxiv.org/abs/1705.05699) [cond-mat.str-el]
- Paddison JAM, Daum M, Dun Z, Ehlers G, Liu Y, Stone MB, Zhou H, Mourigal M (2017) Continuous excitations of the triangular-lattice quantum spin liquid YbMgGaO_4 . *Nat Phys* 13:117–122
- Shen Y, Li Y-D, Walker HC, Steffens P, Boehm M, Zhang X, Shen S, Wo H, Chen G, Zhao J (2018) Fractionalized excitations in the partially magnetized spin liquid candidate YbMgGaO_4 . *Nat Commun* 9:4138

40. Li Y-D, Shen Y, Li Y, Zhao J, Chen G (2018) Effect of spin-orbit coupling on the effective-spin correlation in YbMgGaO_4 . *Phys Rev B* 97:125105
41. Zhang X, Mahmood F, Daum M, Dun Z, Paddison JAM, Laurita NJ, Hong T, Zhou H, Armitage NP, Mourigal M (2018) Hierarchy of exchange interactions in the triangular-lattice spin liquid YbMgGaO_4 . *Phys Rev X* 8:031001
42. Luo Z-X, Lake E, Mei J-W, Starykh OA (2018) Spinon magnetic resonance of quantum spin liquids. *Phys Rev Lett* 120:037204
43. Zhu Z, Maksimov PA, White SR, Chernyshev AL (2017) Disorder-induced mimicry of a spin liquid in YbMgGaO_4 . *Phys Rev Lett* 119:157201
44. Zhu Z, Maksimov PA, White SR, Chernyshev AL (2018) Topography of spin liquids on a triangular lattice. *Phys Rev Lett* 120:207203
45. Maksimov PA, Zhu Z, White SR, Chernyshev AL (2019) Anisotropic-exchange magnets on a triangular lattice: spin waves, accidental degeneracies, and dual spin liquids. *Phys Rev X* 9:021017
46. Kimchi I, Nahum A, Senthil T (2018) Valence bonds in random quantum magnets: theory and application to YbMgGaO_4 . *Phys Rev X* 8:031028
47. Liu C, Yu R, Wang X (2016) Semiclassical ground-state phase diagram and multi- q phase of a spin-orbit-coupled model on triangular lattice. *Phys Rev B* 94:174424
48. Luo Q, Hu S, Xi B, Zhao J, Wang X (2017) Ground-state phase diagram of an anisotropic spin- $\frac{1}{2}$ model on the triangular lattice. *Phys Rev B* 95:165110
49. Li Y-D, Lu Y-M, Chen G (2017) Spinon Fermi surface $U(1)$ spin liquid in the spin-orbit-coupled triangular-lattice Mott insulator YbMgGaO_4 . *Phys Rev B* 96:054445
50. Masaki O (2000) Commensurability, excitation gap, and topology in quantum many-particle systems on a periodic lattice. *Phys Rev Lett* 84:1535–1538
51. Hastings MB (2004) Lieb-schultz-mattis in higher dimensions. *Phys Rev B* 69:104431
52. Lieb E, Schultz T, Mattis D (1961) Two soluble models of an antiferromagnetic chain. *Ann Phys* 16:407–466
53. Watanabe H, Po HC, Vishwanath A, Zaletel M (2015) Filling constraints for spin-orbit coupled insulators in symmorphic and nonsymmorphic crystals. *Proc Natl Acad Sci* 112:14551–14556
54. Liu W, Zhang Z, Ji J, Liu Y, Li J, Wang X, Lei H, Chen G, Zhang Q (2018) Rare-earth chalcogenides: a large family of triangular lattice spin liquid candidates. *Chin Phys Lett* 35:117501
55. Wu C-M, Deng G, Gardner JS, Vorderwisch P, Li W-H, Yano S, Peng J-C, Imamovic E, (2016) SIKa—the multiplexing cold-neutron triple-axis spectrometer at ANSTO. *J Instrum* 11:10009
56. Baenitz M, Schlender P, Sichelschmidt J, Onykieienko YA, Zangeneh Z, Ranjith KM, Sarkar R, Hozoi L, Walker HC, Orain J-C, Yasuoka H, van den Brink J, Klaus HH, Inosov DS, Doert T (2018) NaYbS_2 : a planar spin- $\frac{1}{2}$ triangular-lattice magnet and putative spin liquid. *Phys Rev B* 98:220409
57. Bordelon MM, Kenney E, Liu C, Hogan T, Posthuma L, Kavand M, Lyu Y, Sherwin M, Butch NP, Brown C, Graf MJ, Balents L, Wilson SD (2019) Field-tunable quantum disordered ground state in the triangular-lattice antiferromagnet NaYbO_2 . *Nat Phys* 15:1058–1064
58. Ranjith KM, Dmytrieva D, Khim S, Sichelschmidt J, Luther S, Ehlers D, Yasuoka H, Wosnitza J, Tsirlin AA, Kühne H, Baenitz M (2019) Field-induced instability of the quantum spin liquid ground state in the $J_{\text{eff}} = \frac{1}{2}$ triangular-lattice compound NaYbO_2 . *Phys Rev B* 99:180401
59. Ding L, Manuel P, Bachus S, Grubler F, Gegenwart P, Singleton J, Johnson RD, Walker HC, Adroja DT, Hillier AD, Tsirlin AA (2019) Gapless spin-liquid state in the structurally disorder-free triangular antiferromagnet NaYbO_2 . *Phys Rev B* 100:144432
60. Xing J, Sanjeeva LD, Kim J, Meier WR, May AF, Zheng Q, Custelcean R, Stewart GR, Sefat AS (2019) Synthesis, magnetization, and heat capacity of triangular lattice materials NaErSe_2 and KErSe_2 . *Phys Rev Mater* 3:114413
61. Zangeneh Z, Avdoshenko S, van den Brink J, Hozoi L (2019) Single-site magnetic anisotropy governed by interlayer cation charge imbalance in triangular-lattice AYbX_2 . *Phys Rev B* 100:174436
62. Xing J, Sanjeeva LD, Kim J, Stewart GR, Podlesnyak A, Sefat AS (2019) Field-induced magnetic transition and spin fluctuations in the quantum spin-liquid candidate CsYbSe_2 . *Phys Rev B* 100:220407
63. Ranjith KM, Luther S, Reimann T, Schmidt B, Schlender P, Sichelschmidt J, Yasuoka H, Strydom AM, Skourski Y, Wosnitza J, Kühne H, Doert T, Baenitz M (2019) Anisotropic field-induced ordering in the triangular-lattice quantum spin liquid NaYbSe_2 . *Phys Rev B* 100:224417
64. Sarkar R, Schlender P, Grinenko V, Haeussler E, Baker PJ, Doert T, Klaus HH (2019) Quantum spin liquid ground state in the disorder free triangular lattice NaYbS_2 . *Phys Rev B* 100:241116
65. Xing J, Sanjeeva LD, Kim J, Stewart GR, Du M-H, Reboredo FA, Custelcean R, Sefat AS (2020) Crystal synthesis and frustrated magnetism in triangular lattice CsRESe_2 ($\text{RE} = \text{La-Lu}$): quantum spin liquid candidates CsCeSe_2 and CsYbSe_2 . *ACS Mater Lett* 2:71–75
66. Gao S, Xiao F, Kamazawa K, Ikeuchi K, Biner D, Krämer KW, Rüegg C, Arima T (2020) Crystal electric field excitations in the quantum spin liquid candidate NaErS_2 . *Phys Rev B* 102:024424
67. Scheie A, Garlea VO, Sanjeeva LD, Xing J, Sefat AS (2020) Crystal-field Hamiltonian and anisotropy in KErSe_2 and CsErSe_2 . *Phys Rev B* 101:144432
68. Ma J, Kamiya Y, Hong T, Cao HB, Ehlers G, Tian W, Batista CD, Dun ZL, Zhou HD, Matsuda M (2016) Static and dynamical properties of the spin-1/2 equilateral triangular-lattice antiferromagnet $\text{Ba}_3\text{CoSb}_2\text{O}_9$. *Phys Rev Lett* 116:087201
69. Garlea VO, Sanjeeva LD, McGuire MA, Batista CD, Samarakoon AM, Graf D, Winn B, Ye F, Hoffmann C, Kolis JW (2019) Exotic magnetic field-induced spin-superstructures in a mixed honeycomb-triangular lattice system. *Phys Rev X* 9:011038
70. Wills AS (2000) A new protocol for the determination of magnetic structures using simulated annealing and representational analysis (sarah). *Physica B: Condensed Matter* 276–278:680–681
71. Perez-Mato JM, Gallego SV, Tasci ES, Elcoro L, de la Flor G, Aroyo MI (2015) Symmetry-based computational tools for magnetic crystallography. *Annual Review of Materials Research* 45:217–248
72. Ye M, Chubukov AV (2017) Half-magnetization plateau in a Heisenberg antiferromagnet on a triangular lattice. *Phys Rev B* 96:140406
73. Haley SC, Weber SF, Cookmeyer T, Parker DE, Maniv E, Maksimovic N, John C, Doyle S, Maniv A, Ramakrishna SK, Reyes AP, Singleton J, Moore JE, Neaton JB, Analytis JG (2020) Half-magnetization plateau and the origin of threefold symmetry breaking in an electrically switchable triangular antiferromagnet. *Phys Rev Research* 2:043020
74. Bachus S, Iakovlev IA, Li Y, Wörl A, Tokiwa Y, Ling L, Zhang Q, Mazurenko VV, Gegenwart P, Tsirlin AA (2020) Field evolution of the spin-liquid candidate YbMgGaO_4 . *Phys Rev B* 102:104433
75. Bordelon MM, Liu C, Posthuma L, Kenney E, Graf MJ, Butch NP, Banerjee A, Calder S, Balents L, Wilson SD (2021) Frustrated Heisenberg $J_1 - J_2$ model within the stretched diamond lattice of LiYbO_2 . *Phys Rev B* 103:014420
76. Wawrzyńska E, Coldea R, Wheeler EM, Sörgel T, Jansen M, Ibberson RM, Radaelli PG, Koza MM (2008) Charge disproportionation and collinear magnetic order in the frustrated triangular antiferromagnet AgNiO_2 . *Phys Rev B* 77:094439
77. Coldea A, Seabra L, McCollam A, Carrington A, Malone L, Bangura AF, Vignolles D, van Rhee PG, McDonald RD, Sörgel T, Jansen M, Shannon N, Coldea R (2014) Cascade of field-induced magnetic transitions in a frustrated antiferromagnetic metal. *Phys Rev B* 90:020401
78. Durst AC, Lee PA (2000) Impurity-induced quasiparticle transport and universal-limit Wiedemann-franz violation in d-wave superconductors. *Phys Rev B* 62:1270–1290
79. Dai P-L, Zhang G, Xie Y, Duan C, Gao Y, Zhu Z, Feng E, Tao Z, Huang C-L, Cao H, Podlesnyak A, Granroth GE, Everett MS, Neufeind JC, Voneshen D, Wang S, Tan G, Morosan E, Wang X, Lin H-Q, Shu L, Chen G, Guo Y, Lu X, Dai P (2021) Spinon Fermi surface spin liquid in a triangular lattice antiferromagnet NaYbSe_2 . *Phys Rev X* 11:021044
80. Zhang Z, Li J, Xie M, Zhuo W, Adroja DT, Baker PJ, Perring TG, Zhang A, Jin F, Ji J, Wang X, Ma J, Zhang Q (2021) Low-energy spin dynamics of quantum spin liquid candidate NaYbSe_2 . *cond-mat.str-el*. [arXiv:2112.07199](https://arxiv.org/abs/2112.07199)
81. Zhang Z, Ma X, Li J, Wang G, Adroja DT, Perring TP, Liu W, Jin F, Ji J, Wang Y, Kamiya Y, Wang X, Ma J, Zhang Q (2021) Crystalline electric field excitations in the quantum spin liquid candidate NaYbSe_2 . *Phys Rev B* 103:035144